Journal of Ceramic Processing Research. Vol. 17, No. 9, pp. 919~924 (2016)

J O U R N A L O F
Ceramic Processing Research

High-frequency induction heated sintering of nanostructured WC and WC-$TiAl_3$ hard materials their mechanical properties

In-Jin Shon*

Division of Advanced Materials Engineering, the Research Center of Hydrogen Fuel Cell, Chonbuk National University, 664-14 Deokjin-dong 1-ga, Deokjin-gu, Jeonju, Jeonbuk 561-756, Korea

Tungsten carbides are primarily used as cutting tools and abrasive materials in the form of composites with a binder metal, such as Co or Ni. However, these binder phases have low corrosion resistance compared to the carbide phase and the high cost of Ni or Co. Therefore, the drawbacks of the WC-Ni and WC-Co cermets have generated interest in recent years for alternative binder phases. In this study, $TiAl_3$ was used as a novel binder and consolidated by the high-frequency induction heated sintering (HFIHS) method. The advantage of this process is not only rapid densification to near theoretical density but also the prohibition of grain growth in nano-structured materials. Highly dense WC-$TiAl_3$ with a relative density of up to 98% was obtained within one min by HFIHS under a pressure of 80 MPa. The microstructure and the mechanical properties (hardness and fracture toughness) of the sintered WC and WC-$TiAl_3$ were investigated.

Key words: Nanomaterials, Sintering, Mechanical properties, Hard materials.

Introduction

The attractive properties of tungsten carbides is their high melting point (a peritectic melting temperature of 2785 ºC), high hardness (2854 kg/mm^2), high thermal and electrical conductivities, and relatively high chemical stability [1, 2]. Tungsten carbides are primarily used as cutting tools and abrasive materials in the form of composites with a binder metal, such as Co or Ni. However, these binder phases have inferior chemical characteristics compared to the carbide phase. Most notably, corrosion and oxidation occur preferentially in the binder phase [3]. Hence, the high cost of Ni or Co and the low corrosion resistance of the WC-Ni or WC-Co cermet have generated interest in recent years to find alternative binder phases [4, 5]. It has been reported that aluminides show a higher oxidation resistance, a higher hardness and a cheaper materials compared to Ni or Co [6].

The improvement of mechanical properties and stability of tungsten carbides could be achieved through microstructural changes such as grain size refinement [7, 8]. In this regard, nanostructured materials have received much attention as advanced engineering materials with improved mechanical properties [9, 10]. Since they possess a high strength and hardness as well as excellent ductility and toughness, they have garnered more attention recently. In recent days, nanocrystalline powders have been developed by the thermochemical and thermomechanical process named as the spray conversion process (SCP), co-precipitation and high energy milling [11-13]. High energy ball milling among the methods, the raw powders can be synthesized during the milling [14, 15] and the sintering temperature of high energy mechanically milled powder is lower than that of unmilled powder due to the increased reactivity, internal and surface energies, and surface area of the milled powder, which contribute to its so-called mechanical activation [16-18]. However, the grain size in sintered materials becomes much larger than that in pre-sintered powders due to a rapid grain growth during a conventional sintering process. Therefore, even though the initial particle size is less than 100 nm, the grain size increases rapidly up to 2 μm or larger during conventional sintering [19]. So, controlling grain growth during sintering is one of the keys to the commercial success of nanostructured materials. In this regard, the pulsed current activated sintering method which can make dense materials within 2 min, has been shown to be effective in achieving this goal [20-22].

The purpose of this work is to produce dense nanocrystalline WC, WC-5 vol.% $TiAl_3$ and WC-10 vol.% $TiAl_3$ hard materials within one min from mechanically milled powders using this high-frequency induction heated sintering method and to evaluate its mechanical properties and microstructure.

Experimental Procedures

The WC powder used in this study was supplied by Taegu Tec company (Korea). The average particle size

*Corresponding author:
Tel : +82-63-270-2381
Fax: +82-63-270-2386
E-mail: ijshon@chonbuk.ac.kr

was about 0.5 μm and the purity was 99.8%. $TiAl_3$ (-325 mesh, 99% pure, Sejong Co.) was used as binder material. Powders of two compositions corresponding to WC, WC-5 vol.% $TiAl_3$ and WC-10 vol.%$TiAl_3$ were prepared by weighting and milled in a high-energy ball mill (Pulverisette-5 planetary mill) at 250 rpm for 20 h. WC balls (10 mm in diameter) were used in a sealed cylindrical stainless steel vial under an argon atmosphere. The weight ratio of balls-to-powder was 25 : 1. The grain size of the powders was calculated from the full width at half-maximum (FWHM) of the diffraction peak by Suryanarayana and Grant Norton's formula [23].

$$B_r(B_{crystalline} + B_{strain}) \cos\theta = k\,\lambda / L + \eta\sin\theta \quad (1)$$

where B_r is the full width at half-maximum (FWHM) of the diffraction peak after instrumental correction; $B_{crystalline}$ and B_{strain} are FWHM caused by small grain size and internal stress, respectively; k is constant (with a value of 0.9); λ is wavelength of the X-ray radiation; L and η are grain size and internal strain, respectively; and θ is the Bragg angle. The parameters B and B_r follow Cauchy's form with the relationship: $B = B_r + B_s$, where B and B_s are the FWHM of the broadened Bragg peaks and the standard sample's Bragg peaks, respectively.

The milled powders were placed in a graphite die (outside diameter, 45 mm; inside diameter, 20 mm; height, 40 mm) and then introduced into the induced current activated sintering (HFIH) system made by Eltek Co in the Republic of Korea. A schematic diagram of this system is shown in Ref. [24-26]. The PCAS apparatus includes a 15 kW power supply and a uniaxial press with a maximum load of 50 kN. The system was first evacuated and a uniaxial pressure of 80 MPa was applied. A induced current was then activated and maintained until the densification rate became negligible, as indicated by the observed shrinkage of the sample. Sample shrinkage was measured in real time by a linear gauge measuring the vertical displacement. Temperature was measured by a pyrometer focused on the surface of the graphite die. At the end of the process, the current was turned off and the sample was allowed to cool to room temperature. The entire process of densification using the HFIHS technique consists of four major control stages: chamber evacuation, pressure application, power application, and cooling off. The process was carried out under a vacuum of 12 Pa.

The relative densities of the sintered samples were measured by the Archimedes method. Microstructural information was obtained from the product samples, which had been polished and etched, using Murakami's reagent (10 g potassium ferricyanide, 10 g sodium hydroxide, and 100 ml water), for 1-2 minutes at room temperature. Compositional and microstructural analyses of the samples were carried out through X-ray diffraction (XRD), and field-emission scanning electron microscopy (FE-SEM). Vickers hardness was measured by performing indentations at a load of 20 kg_f with a dwell time of 15 s.

Results and Discussion

Fig. 1 shows FE-SEM images of WC, WC-5 vol.% $TiAl_3$ and WC-10 vol.%$TiAl_3$ powders milled for 20 h. The powders have nano-size and some agglomeration. X-ray diffraction pattern of the WC, WC-5 vol.% $TiAl_3$ and WC-10 vol.%$TiAl_3$ powders after milling for 20 h are shown in Fig. 2. The broadening of WC peaks due to crystallite refinement and strain is evident after milling for 20 h. The milling process is known to introduce impurities from the ball and/or container. However, in this study, peaks other than WC were not identified. Fig. 3 shows plot of $B_r(B_{crystalline} + B_{strain})$ cosè versus sinθ in Suryanarayana and Grant Norton's formula [23] to calculate particle size. The average

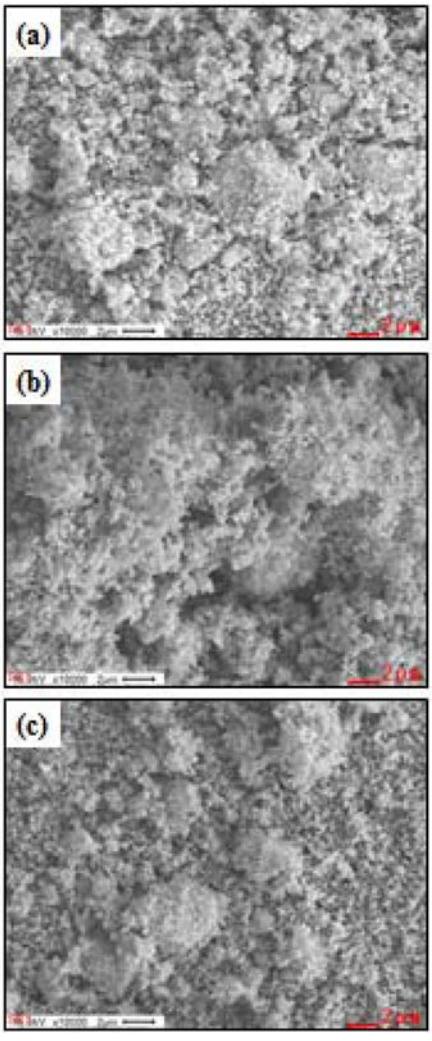

Fig 1. FE-SEM images of powders milled for 20 h; (a) WC, (b) WC-5 vol.%$TiAl_3$ and (c) WC-10 vol.%$TiAl_3$.

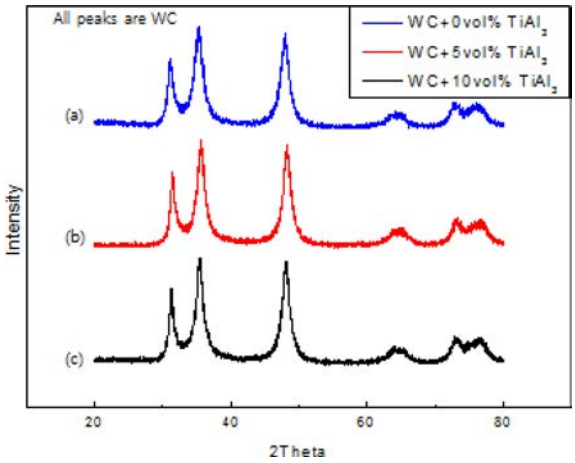

Fig. 2. XRD patterns of (a) WC, (b) WC-5 vol.%$TiAl_3$ (c) WC-10 vol% $TiAl_3$ powders milled for 20 h.

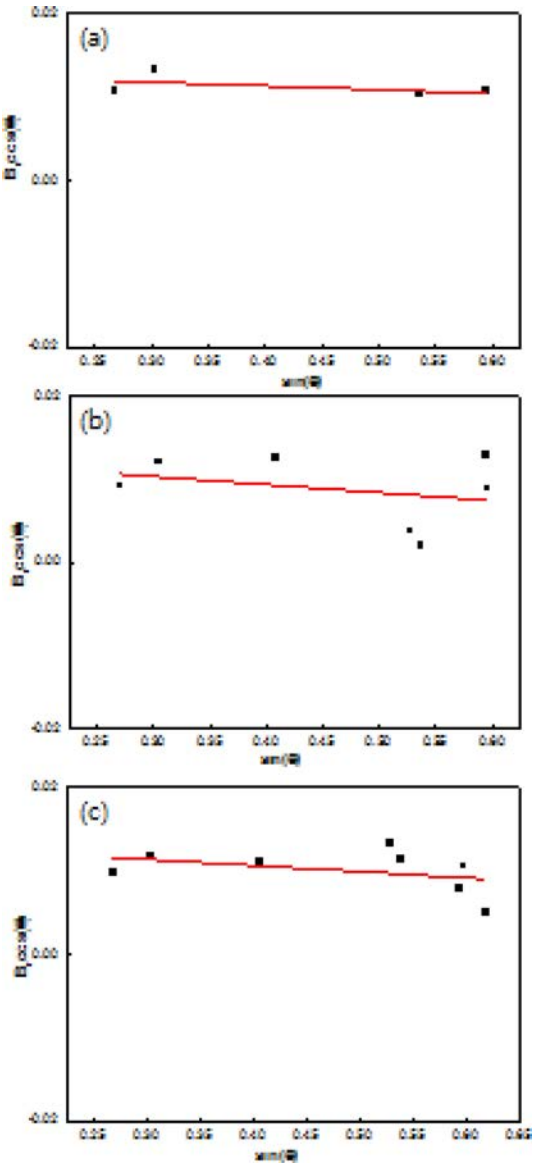

Fig. 3. Plot of Br ($B_{crystalline} + B_{strain}$) cosè versus sinè for WC in (a) WC, (b) WC-5 vol.%$TiAl_3$ and (c) WC-10 vol.%$TiAl_3$ powders milled for 20 h.

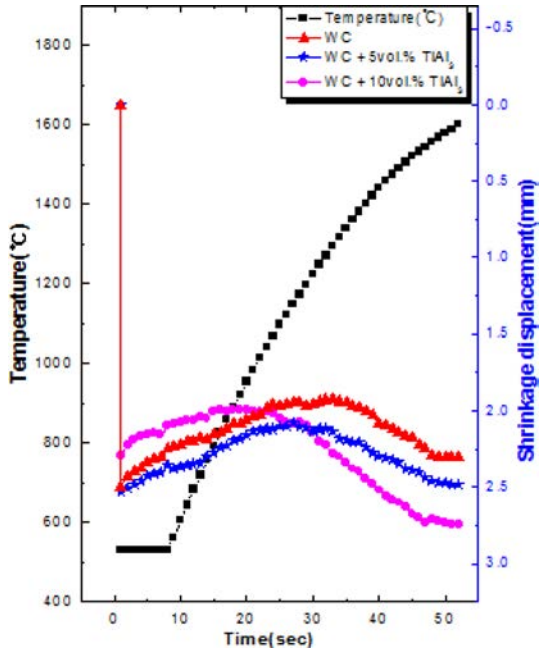

Fig. 4. Variation of temperature and shrinkage with heating time during the sintering of WC, WC-5 vol.%$TiAl_3$ and WC-10 vol.%$TiAl_3$.

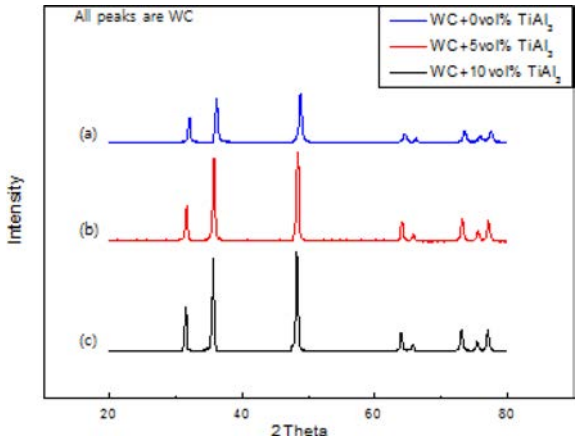

Fig. 5. XRD patterns of (a) WC (b) WC-5 vol.%$TiAl_3$ and (c) WC-10 vol.%$TiAl_3$ hard materials produced by HFIHS.

grain sizes of the WC in the WC, WC-5 vol.% $TiAl_3$ and WC-10 vol.% $TiAl_3$ powders after milling for 20 h. calculated from the XRD data were about 11,10 and 10 nm, respectively.

Fig. 4 shows the variations in shrinkage displacement and temperature of the surface of the graphite die with heating time during the processing of WC, WC-5 vol.% $TiAl_3$ and WC-10 vol.%$TiAl_3$ powders. The application of the induced current resulted in shrinkage due to consolidation. As the induced current was applied, the thermal expansion showed and then the shrinkage displacement abruptly increased. The temperature of abrupt shrinkage was reduced remarkably by the addition of $TiAl_3$. So, it is expected that $TiAl_3$ would be molten during the sintering process. The main densification

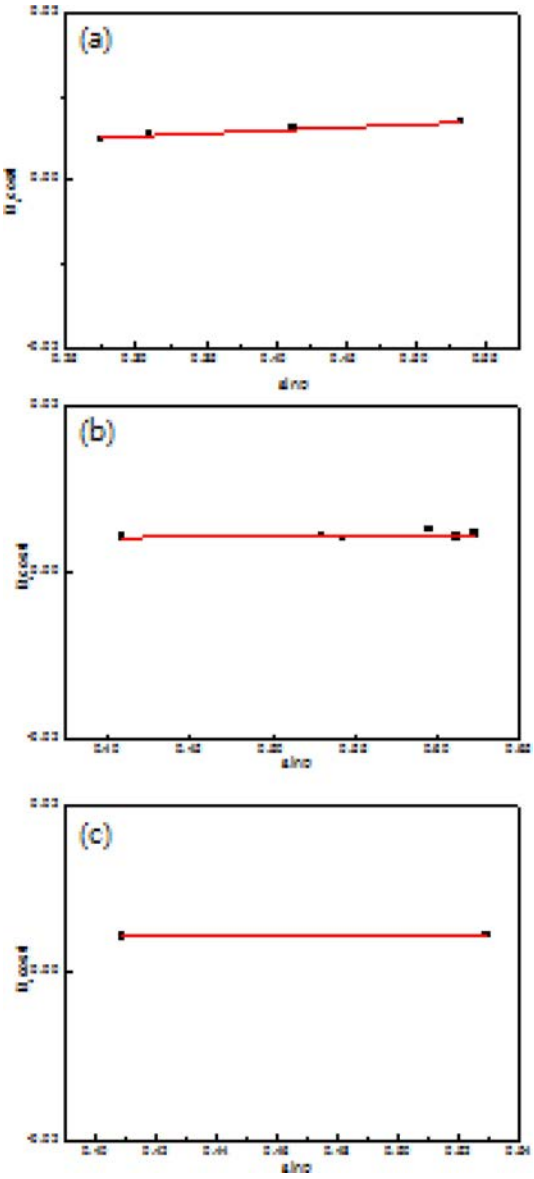

Fig. 6. Plot of Br ($B_{crystalline} + B_{strain}$) cosθ versus sinθ for WC in (a)WC, (b) WC-5 vol.%$TiAl_3$ and (c) WC-10 vol.%$TiAl_3$ sintered by HFIHS.

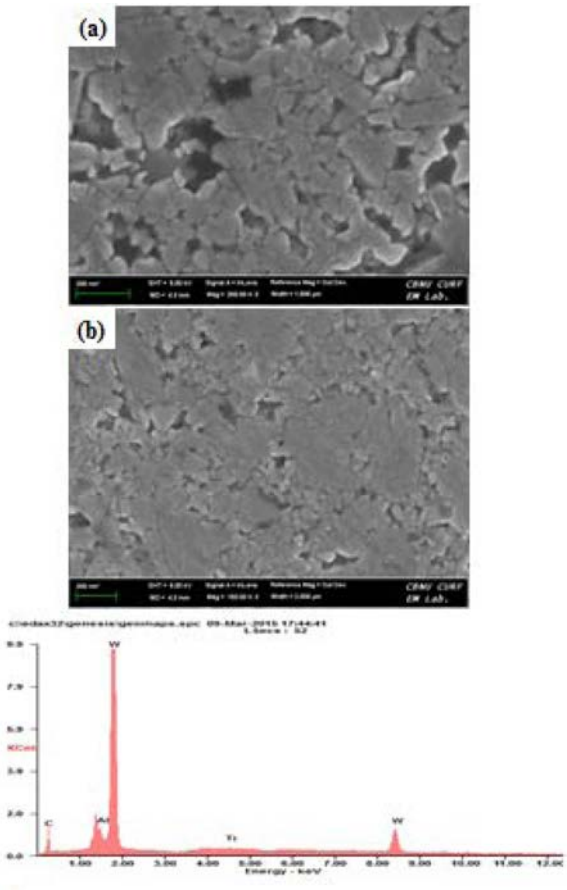

Fig. 7. FEM images and EDS of (a) WC, (b) WC-10vol.%$TiAl_3$ hard materials produced by HFIHS.

mechanism for this is the rearrangement of carbide particles, enhancement of the diffusion, and viscous flow of the binder [27].

And the shrinkage displacement gradually increased with temperature up to about 1320 ºC. Fig. 5 shows the XRD patterns of WC, WC-5 vol.% $TiAl_3$ and WC-10 vol.%$TiAl_3$ sintered at 1600 ºC. In all cases, only WC peaks are detected. Plot of B_r ($B_{crystalline} + B_{strain}$) cosè versus sinè in Suryanarayana and Grant Norton's formula [23] to calculate grain size of WC in sintered samples is shown in Fig. 6. The average grain sizes of the WC calculated from the XRD data using Suryanarayana and Grant Norton's formula are about 44, 42 and 40 nm for the samples with WC, WC-5 vol.% $TiAl_3$ and WC-10 vol.% $TiAl_3$. Fig. 7 shows FE-SEM images and EDS of the samples after being sintered up to 1600 ºC. It is apparent that the WC grains consist of nanocrystallites suggesting the absence of grain growth during sintering. This retention of the fine grain structure can be attributed to the high heating rate and the relatively short exposure to the high temperature. In EDS, W, C, Ti and Al in sintered WC-10 vol%$TiAl_3$ were detected. And there are no other peaks, such as Fe, which can possibly happen during the milling process. Relative densities corresponding to WC, WC-5 vol.% $TiAl_3$ and WC-10vol.%$TiAl_3$ were approximately 98, 98.5 and 99%, respectively.

The role of the current in sintering has been the focus of several attempts to provide an explanation for the observed sintering enhancement and the improved characteristics of the products. The role played by the current has been variously interpreted. The effect has been explained by fast heating due to Joule heating at contacts points [28], the presence of plasma in pores separating powder particles, and the intrinsic contribution of the current to fast mass transport [29].

Vickers hardness measurements were performed on polished sections of the WC, WC-5 vol.% $TiAl_3$ and WC-10 vol.%$TiAl_3$ samples using a 20 kg load and 15 s dwell time. Indentions with 20 kgf load produced median cracks around the indentation from which

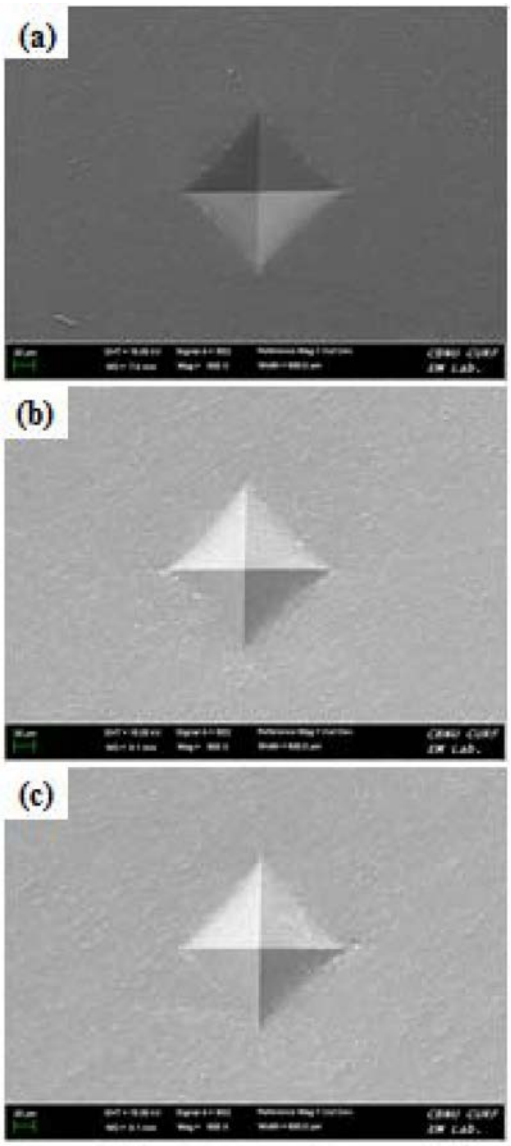

Fig. 8. Vickers hardness indeatation in (a)WC (b) WC-5 vol. %$TiAl_3$ and (c) WC-10 vol.%$TiAl_3$ hard materials produced by HFIHS.

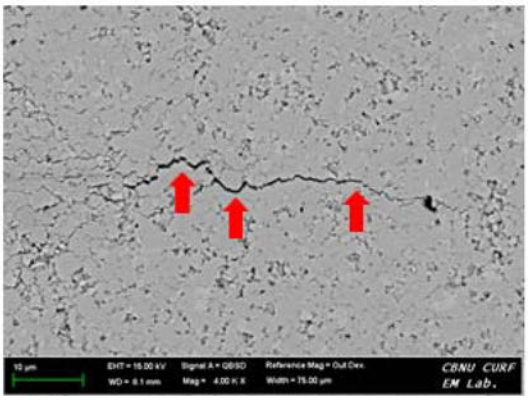

Fig. 9. Crack propagation in WC-10 Vol% $TiAl_3$ hard materials produced by HFIHS.

fracture toughness can be calculated. The lengths of these cracks permit estimation of the fracture toughness of the materials by means of the expression [30]:

$$K_{IC} = 0.023(c / a)^{-3/2} \cdot H_v \cdot a^{1/2} \quad (2)$$

where c is the trace length of the crack measured from the center of the indentation, a is one half of the average length of the two indent diagonals, and H_v is the hardness.

The Vickers hardness and the fracture toughness values of the WC, WC-5 vol.% $TiAl_3$ and WC-10vol.%$TiAl_3$ samples were 2810 kg/mm^2, 6.1 MPa · m$^{1/2}$ and 2710 kg/mm^2, 8 MPa · m$^{1/2}$ and 2685 kg/mm^2, 9.7 MPa · m$^{1/2}$, respectively. These values represent the average of five measurements. The fracture toughness of WC-5 vol.% $TiAl_3$ and WC-10 vol.%$TiAl_3$ samples are higher than that of monolithic WC without great decrease of hardness because the grain size of WC decreases with addition of $TiAl_3$. The sintering method in this study was proven to be very effective to consolidate WC-$TiAl_3$ cermets. In one of the reported studies [31], WC-10Co and WC-10Ni were consolidated at 1250 ºC by high-frequency induction heated sintering. Comparing this investigation of WC-10 vol.%$TiAl_3$ with a study of WC-10Co and WC-10Ni [31], there is a little difference in fracture toughness but hardness in this study is higher than that in the other study [31]. The use of $TiAl_3$ binder instead of Co or Ni is very effective especially to maintain the high hardness of monolithic WC without the expense of toughness reduction. In this regard, it would be worthwhile to consider $TiAl_3$ as the possible replacement for Co or Ni especially for the applications requiring a high hardness.

Vickers hardness indentations in the WC, WC-5 vol.%$TiAl_3$ and WC-10 vol.%$TiAl_3$ samples are shown in Fig. 8. They show typically one to three additional cracks propagating radially from the indentation. Fig. 9 shows a crack propagated in a deflective and branching manner (↑) in WC-10 vol.%$TiAl_3$ composite. The enhanced fracture toughness of WC-10 vol.%$TiAl_3$ composite is believed that WC and $TiAl_3$ in the composite may deter the propagation of cracks and WC and $TiAl_3$ have nanostructure phases.

Conclusions

WC nanopowders were fabricated using high energy ball milling. Using high-frequency induction heated sintering (HFIHS), the rapid consolidation of the WC, WC-5 vol.%$TiAl_3$ and WC-10 vol.%$TiAl_3$ was accomplished successfully. Nearly full-dense nanostructured WC, WC-5 vol.%$TiAl_3$ and WC-10 vol.%$TiAl_3$ composite could be obtained within one min. The densification temperature of WC was reduced remarkably by the addition of $TiAl_3$. The average grain sizes of the WC are about 44, 42 and 40 nm for the samples with WC, WC-5vol.%$TiAl_3$ and WC-10 vol.%$TiAl_3$. The Vickers hardness and the fracture toughness values of the WC, WC-5 vol.%$TiAl_3$ and WC-10 vol.%$TiAl_3$ samples were

2810 kg/mm^2, 6.1 MPa · m$^{1/2}$ and 2710 kg/mm^2, 8 MPa · m$^{1/2}$ and 2685 kg/mm^2, 9.7 MPa · m$^{1/2}$, respectively. The addition of $TiAl_3$ to WC improved the fracture toughness of cemented WC without great reduction of hardness.

Acknowledgments

This work was supported by a grant in aid awarded by the Basic Research Project of the Korea Institute of Geoscience and Mineral Resources (KIGAM), funded by the Ministry of Science, ICT and Future Planning (GP2015036) and this research was supported by Basic Science Research Program though the National Research Foundation of Korea (NRF) funded by the Ministry of Education (2015R1D1A1A01056600) and this work was supported by the Korea Institute of Energy Technology Evaluation and Planning(KETEP) and the Ministry of Trade, Industry & Energy(MOTIE) of the Republic of Korea (No. 20164030201070).

References

1. H. C. Kim, I. J. Shon, I. K. Jeong, I. Y. Ko, J. K. Yoon, J. M. Doh, Metals and Materials International, Vol. 13 (2007) 39-45.
2. H. Suzuki, Cemented Carbide and Sintered Hard Materials, Maruzen, Tokyo (1986) 262-268.
3. S. Imasato, K. Tokumoto, T. Kitada, S. Sakaguchi, Int J of Refract Met and Hard Mater. 13 (1995) 305-12.
4. G. Gille, J. Bredthauer, B. Gries, B. Mende, Int J of Refract Met and Hard Mater. 18[2-3] (2000) 87-102.
5. Hua Lin, Bowan Tao, Jie Xiong, Qing Li , Int. Journal of Refractory Metals and Hard Materials, 41 (2013) 363-365.
6. Z.G. Zhang, F. Gesmundo, P.Y. Hou, Y. Niu, Corrosion Science, 48 (2006) 741-765.
7. H Gleiter, Nanocrystalline materials, Progress in Materials Science, 33[4] (1989) 223-315.
8. GE Fougere, JR Weertman, RW Siegel, S Kim, Scripta Metallurgica et Materialia 26 [2] (1992) 1879-1883.
9. M. Sherif El-Eskandarany, J. Alloys & Compounds, 305 (2000) 225-38.
10. L Fu, LH Cao, YS Fan, Scripta Materialia, 44 (2001) 1061-1068.
11. Z. Fang, J.W. Eason, Int. J. Refract. Met. Hard Mater. 13 (1995) 297-303.
12. A.I.Y. Tok, L.H. Luo, F.Y.C. Boey, Mater. Sci. Eng. A. 383 (2004) 229-234.
13. I.J. Shon, H.G. Jo, H.J. Kwon, Korean J. Met. Mater. 52 (2014) 343-346.
14. I.J. Shon, H.G. Jo, B.S. Kim, J.K. Yoon, K.T. Hong, Korean J. Met. Mater. 53 (2015) 474-479.
15. S.M. Kwon, N.R. Park, J.W. Shin, S.H. Oh, B.S. Kim, I.J. Shon, Korean J. Met. Mater. 53 (2015) 555-562.
16. B.R. Kang, J.K. Yoon, K.T. Hong, I.J. Shon, Met. Mater. Int. 21 (2015) 698-703.
17. B.R. Kang and I.J. Shon, Korean J. Met. Mater. 53 (2015) 320-325.
18. H.S. Kang and I.J. Shon, Korean J. Met. Mater. 52 (2014) 623-629.
19. J. Jung, S. Kang, Scripta Mater. 56 (2007) 561-564.
20. Bong-Won Kwak, Byung-Su Kim, Jin-Kook Yoon, Kyung-Tae Hong and In-Jin Shon, Journal of Ceramic Processing Research. Vol. 16, No. 3 (2015) 340-345.
21. H.S. Kang, S.L. Du, J.M. Doh, J.K. Yoon, I.J. Shon, Electron. Mater. Lett. 10 (2014) 529-533.
22. I.J. Shon, Korean J. Met. Mater. 52 (2014) 573-580.
23. Suryanarayana C. and Grant Norton M., *X-ray Diffraction A Practical Approach*, Plenum Press, New York, 1998.
24. In-Jin Shon, Hyun-Su Kang, Jung-Mann Doh, and Jin-Kook Yoon, Met. Mater. Int. 21 (2015) 345-349.
25. In-Jin Shon, Hanjung Kwon, and Hyun-Su Oh, Electron. Mater. Lett. 10 (2014) 337-343.
26. Hyun Su Kang, Jung Mann Doh, Jin Kook Yoon, and In Jin Shon, Korean J. Met. Mater. 52 (2014) 759-764.
27. GS Upadhyaya, Materials & Design 22[6] (2001) 483-489.
28. Z. Shen, M. Johnsson, Z. Zhao and M. Nygren, Spark plasma sintering of alumina, J. Am. Ceram. Soc. 85 (2002) 1921-1927.
29. J. E. Garay, U. Anselmi-Tamburini, Z. A. Munir, S. C. Glade and P. Asoka- Kumar, Appl. Phys. Lett. 85 (2004) 573-575.
30. K. Niihara, R. Morena, and D. P. H. Hasselman, J. Mater. Sci. Lett. 1 (1982) 12-16.
31. In-Jin Shon, In-Kyoon Jeong, In-Yong Ko, Jung-Mann doh, Kee-Do Woo, Ceramics International 35 (2009) 339-344.